Multiscale Finite Element Method for Ventilation Panels

M. Leumüller[1] and K. Hollaus[1,2]

[1]Institute for Analysis and Scientific Computing, Technische Universität Wien, 1040 Vienna, Austria
[2]Coexistence and Electromagnetic Compatibility, Silicon Austria Labs GmbH, 8010 Graz, Austria

In the context of electromagnetic compatibility ventilation panels with small quasi-periodic openings exist. The standard finite element (FE) method leads to a large number of unknowns for ventilation panels. An efficient multiscale FE approach is introduced to cope with the multiple scale problem. To this end, special functions are computed by solving cell problems for a single aperture with FEs of higher order to enhance the FE space. The proposed technique is able to cope with varying thicknesses of the metallic sheet of the ventilation panel and arbitrary shapes of apertures, as well as lossy materials and frequencies in a wide range. The introduced method improves essentially the accuracy of coarse FE simulations for ventilation panels in 3-D.

***Index Terms*— Electromagnetic compatibility, electromagnetic shielding, multiscale finite element method (MSFEM), ventilation panels.**

I. Introduction

In THE context of electromagnetic compatibility metallic ventilation panels, also called metascreens [1], exist, see Fig. 1. These are especially interesting in the case of closed boxes for shielding, because due to, e.g., heat development openings for ventilation need to be incorporated. On the other hand, the shielding property cannot be neglected due to interference with other electronic-based systems. Therefore, the fields transmitted through the ventilation panel are of great interest. Due to the small scale behavior of electromagnetic fields around the apertures usually fine meshes are needed, leading to large systems of linear equations in the finite element method (FEM). A method based on shell elements for periodic structures is presented in [2].

Instead of using a very fine discretization around the apertures a multiscale (MS) approach is chosen such that the MS functions reflect the local behavior in a sufficient way to accurately represent the fields around apertures [3]. Due to the quasi-periodic structure the MS functions need to be calculated only for one aperture. Calculating the MS functions is part of the proposed method and no *a priori* knowledge or analytic approach is required. A MS method for a 2-D ventilation panel without considering lossy materials has been presented in [4].

The considered model problem is introduced in Section II. The MS FEM (MSFEM) is introduced in Section III and the calculation of the MS functions is described in detail in Section IV. The introduced method is applied to ventilation panels with multiple apertures. Numerical results are presented in Section V.

II. Model Description

A 3-D ventilation panel with $N \times M$ apertures is considered, see Fig. 2. The apertures lie in the center of the problem domain. The domain

$$\Omega = \Omega_0 \cup \Omega_{\text{cells}} \tag{1}$$

is decomposed into the exterior domain

$$\Omega_0 = \Omega_{0,a} \cup \Omega_{0,p} \cup \Omega_{0,b} \tag{2}$$

with the domain above the panel $\Omega_{0,a}$, the panel $\Omega_{0,p}$ and the domain below the panel $\Omega_{0,b}$ and the cell domains

$$\Omega_{\text{cells}} := \bigcup_{i=1}^{N} \bigcup_{j=1}^{M} \Omega_{i,j} \tag{3}$$

where for one cell

$$\Omega_{i,j} = \Omega_{i,j,a} \cup \Omega_{i,j,p} \cup \Omega_{i,j,b} \tag{4}$$

holds. Each cell domain represents a single aperture inside the domain. Additionally, all cell domains are geometrically identical up to translation. This property will be called quasi-periodic in this work.

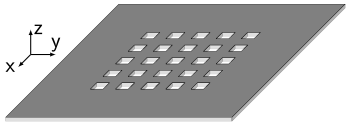

Fig. 1. Ventilation panel with small, quasi-periodic, square apertures.

On the outer boundary Γ_{ABC} below the panel a first-order absorbing boundary condition (ABC) is prescribed [5]. Above the panel plane waves impinging in the directions of the wave vector

$$\mathbf{k} := (0, k_y, k_z)^\top = (0, \sin\alpha, -\cos\alpha)^\top, \quad \alpha \in [0^\circ, 90^\circ] \tag{5}$$

with the electric field parallel to the x-axis are considered as excitations. The angle between the direction of the plane wave and the z-axis is α. An angle of $\alpha = 0^\circ$ represents a plane wave impinging from above and $\alpha = 90^\circ$ represents a plane wave impinging from the front. Homogeneous Dirichlet boundary conditions (DBCs) are considered on Γ_{PEC}. ABCs supporting plane waves impinging at an oblique angle α are

Manuscript received 10 February 2022; revised 1 April 2022; accepted 26 April 2022. Date of publication 28 April 2022; date of current version 26 August 2022. Corresponding author: M. Leumüller (e-mail: michael.leumueller@tuwien.ac.at).

Color versions of one or more figures in this article are available at https://doi.org/10.1109/TMAG.2022.3171098.

Digital Object Identifier 10.1109/TMAG.2022.3171098

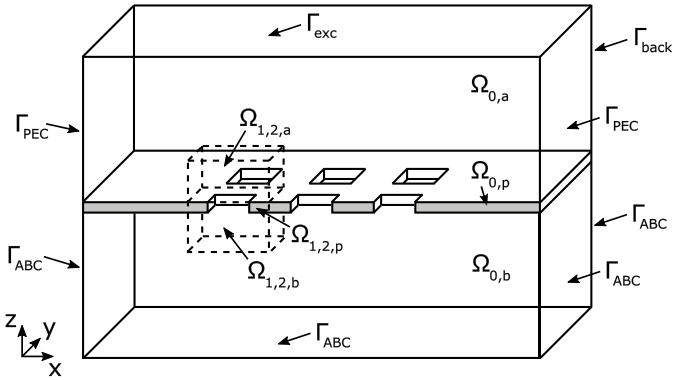

Fig. 2. Geometry with boundaries and subdomains of a ventilation panel with 3×3 apertures. Only one half of the problem is shown. The subdomains $\Omega_{1,2,a}, \Omega_{1,2,p}$ and $\Omega_{1,2,b}$ of the cell domain $\Omega_{1,2}$ are illustrated by dashed lines.

set on Γ_{exc}, Γ_{front}, and Γ_{back}. The plane waves are excited by Neumann boundary conditions (NBCs) prescribed on Γ_{exc}.

Maxwell's equations for the time harmonic case with a magnetic vector potential $\mathbf{A}$ are considered in the entire domain. The boundary value problem reads as: Find $\mathbf{A}$ so that

$$\begin{aligned}
\text{curl}\mu^{-1}\text{curl}\mathbf{A} - \kappa^2\mathbf{A} &= \mathbf{0} \quad \text{in} \quad \Omega \\
\mu^{-1}\text{curl}\mathbf{A} \times \mathbf{n} + \frac{j\omega}{Z_0}(\mathbf{n} \times \mathbf{A}) \times \mathbf{n} &= \mathbf{0} \quad \text{on} \quad \Gamma_{\text{ABC}} \\
\mathbf{A} \times \mathbf{n} &= \mathbf{0} \quad \text{on} \quad \Gamma_{\text{PEC}} \\
\mu^{-1}\text{curl}\mathbf{A} \times \mathbf{n} - k_y\frac{j\omega}{Z_0}(\mathbf{n} \times \mathbf{A}) \times \mathbf{n} &= \mathbf{0} \quad \text{on} \quad \Gamma_{\text{front}} \\
\mu^{-1}\text{curl}\mathbf{A} \times \mathbf{n} + k_y\frac{j\omega}{Z_0}(\mathbf{n} \times \mathbf{A}) \times \mathbf{n} &= \mathbf{0} \quad \text{on} \quad \Gamma_{\text{back}} \\
\mu^{-1}\text{curl}\mathbf{A} \times \mathbf{n} + k_z\frac{j\omega}{Z_0}(\mathbf{n} \times \mathbf{A}) \times \mathbf{n} &= 2\mathbf{h} \times \mathbf{n} \quad \text{on} \quad \Gamma_{\text{exc}} \quad (6)
\end{aligned}$$

where $\kappa^2 = \omega^2\varepsilon - j\omega\sigma$ is the given complex conductivity with the angular frequency $\omega = 2\pi f$, f is the frequency, ε is the permittivity, j is the imaginary unit, σ is the electrical conductivity, μ is the permeability, $Z_0 = (\mu_0/\varepsilon_0)^{1/2}$ is the impedance, $\mathbf{n}$ is the outward pointing normal vector and

$$\mathbf{h}(\mathbf{k}) = k_z\frac{j\omega}{Z_0}\mathbf{n} \times (1, 0, 0)^\top \quad (7)$$

is the excitation, where the magnitude of the incident wave is one.

III. MS Finite Element Method

The usual way to solve the boundary value problem (6) with FEM is to look for a discrete solution $\mathbf{A}_S$ [6] in

$$\text{H}(\text{curl}, \Omega) := \{\mathbf{v} \in [\text{L}^2(\Omega)]^3; \text{curl}\ \mathbf{v} \in [\text{L}^2(\Omega)]^3\}. \quad (8)$$

This would lead to a large number of unknowns, due to the small-scale behavior of the traveling wave through the openings. To keep the number of unknowns relatively small and at the same time to consider the wave propagation through the shielding accurately, the coarse finite element (FE) space is enriched by vector-valued MS functions $\mathbf{S}_i, i \in \{1, \ldots, L\}$ in the MSFEM. Thus, a MS approach

$$\mathbf{A}_{\text{MS}} = \mathbf{A}_S + \sum_{i=1}^{L} c_i\mathbf{S}_i \quad (9)$$

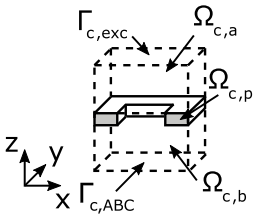

Fig. 3. Geometry, boundaries, and subdomains of the cell domain around the aperture.

with complex coefficients $c_i \in \mathbb{C}$ is considered. The MS functions should enhance the solution by incorporating the transmitted parts of the field through the panel which is not resolved by the coarse FE space. Two MS functions $\mathbf{S}_{i,j,1}$ and $\mathbf{S}_{i,j,2}$ are used per aperture defined in the subdomains $\Omega_{i,j}$, thus $L = 2\,MN$ in total. The MS functions for different cells are identical up to a translation due to the quasi-periodicity of the apertures and only need to be calculated on a single reference cell which can be seen in Fig. 3.

IV. MS Functions

The additional MS functions should improve the transmitted and reflected field at the aperture, therefore it is natural to consider cell solutions $\mathbf{A}_i$ of the following boundary value problem on the cell domain Ω_c, see Fig. 3: Find $\mathbf{A}_i$ so that

$$\begin{aligned}
\text{curl}\mu^{-1}\text{curl}\mathbf{A}_i - \kappa^2\mathbf{A}_i &= \mathbf{0} \quad \text{in} \quad \Omega_c \\
\mu^{-1}\text{curl}\mathbf{A}_i \times \mathbf{n} + \frac{j\omega}{Z_0}(\mathbf{n} \times \mathbf{A}_i) \times \mathbf{n} &= \mathbf{0} \quad \text{on} \quad \Gamma_{c,\text{ABC}} \\
\mu^{-1}\text{curl}\mathbf{A}_i \times \mathbf{n} + \frac{j\omega}{Z_0}(\mathbf{n} \times \mathbf{A}_i) \times \mathbf{n} &= 2\mathbf{h}_i \times \mathbf{n} \quad \text{on} \quad \Gamma_{c,\text{exc}}. \quad (10)
\end{aligned}$$

The domain Ω_c is geometrically identical to the cell domains $\Omega_{i,j}$. ABCs are used on $\Gamma_{c,\text{ABC}}$ below the panel and on $\Gamma_{c,\text{exc}}$ for the scattered field. The plane waves are excited through a NBC on $\Gamma_{c,\text{exc}}$. Two plane waves

$$\mathbf{h}_1 = \frac{j\omega}{Z_0}(1, 0, 0)^\top, \quad \mathbf{h}_2 = \frac{j\omega}{Z_0}(0, 1, 0)^\top \quad (11)$$

with a magnitude of one, are chosen as excitations, thus $\mathbf{A}_1$ and $\mathbf{A}_2$ represent the reflection and transmission of these plane waves on the aperture. Suitable boundary conditions are required for each excitation. In particular, for the excitation $\mathbf{h}_1$ homogenous DBCs are set on $\Gamma_{c,\text{left}}$, $\Gamma_{c,\text{right}}$ and homogenous NBCs are set on $\Gamma_{c,\text{front}}$, $\Gamma_{c,\text{back}}$. For $\mathbf{h}_2$ the boundary conditions are exchanged. Due to the symmetry of the aperture the solutions $\mathbf{A}_1$ and $\mathbf{A}_2$ only differ by a rotation of 90° around the z-axis.

In contrast to the FEM solution on the whole domain Ω, solving for $\mathbf{A}_i$ with FEM can be done with a much higher accuracy, due to the fact that Ω_c is much smaller than Ω.

The solutions $\mathbf{A}_i$ cannot be directly translated to the domains $\Omega_{i,j}$ and used as the MS functions, because the tangential continuity of the solution $\mathbf{A}_{\text{MS}}$ would be broken on the interfaces $\partial\Omega_{i,j}$ and therefore $\mathbf{A}_{\text{MS}} \notin \text{H}(\text{curl}, \Omega)$. To ensure the continuity the cell solutions $\mathbf{A}_i \in \text{H}(\text{curl}, \Omega_c)$ are projected into

$$\text{H}_0(\text{curl}, \Omega_c) := \{\mathbf{v} \in \text{H}(\text{curl}, \Omega_c); \mathbf{v} \times \mathbf{n} = \mathbf{0} \text{ on } \partial\Omega_c\} \quad (12)$$

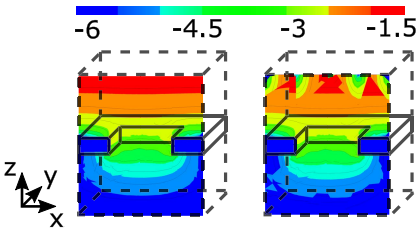

Fig. 4. Magnitude of the cell solution $\mathbf{A}_1$ (left) and magnitude of the MS function $\mathbf{S}_1$ (right) at the frequency $f = 1$ GHz, logarithmically scaled. The cell solution $\mathbf{A}_2$ and MS function $\mathbf{S}_2$ are similar with a 90° rotation around the z-axis.

setting the tangential components on the boundary $\partial\Omega_c$ to zero [6]. Therefore, $\mathbf{S}_i := P(\mathbf{A}_i)$ with a projection

$$P : \mathrm{H}(\mathrm{curl}, \Omega_c) \to \mathrm{H}_0(\mathrm{curl}, \Omega_c). \tag{13}$$

In this work coefficients, corresponding to FE basis functions with nonzero tangential fields on the boundary, are set to zero in the cell solutions. The cell solution $\mathbf{A}_1$ and the MS function $\mathbf{S}_1$ are shown in Fig. 4. The disturbances in $\mathbf{S}_1$ on $\partial\Omega_c$ are due to the projection. The MS function is not smooth, but tangentially continuous. These MS functions are translated into the cell domains, so that

$$\mathbf{S}_{i,j,1} = T_{i,j}(P(\mathbf{A}_1)) \tag{14}$$

with a translation

$$T_{i,j} : \mathrm{H}_0(\mathrm{curl}, \Omega_c) \to \mathrm{H}_0(\mathrm{curl}, \Omega_{i,j}). \tag{15}$$

Although $L = 2MN$ MS functions are needed, only two have to be calculated due to the quasi-periodicity.

V. Numerical Example

The introduced method has been applied to a ventilation panel with $N \times M = 5 \times 5$ apertures. Material parameters representing air have been chosen above and below the panel as well as in the aperture. The panel itself has been considered as a copper sheet and has a thickness of $d = 1$ mm and the width of the square aperture is $s = 4$ mm. The dimensions of the whole domain Ω are $(24+8\,N)$ mm $\times$ $(24+8\,M)$ mm $\times$ 25 mm and the dimensions of the cell domains $\Omega_{i,j}$ are 8 mm $\times$ 8 mm $\times$ 9 mm.

The used reference solutions $\mathbf{A}_{\mathrm{ref}}$ have been calculated by solving (6) with FEM of order $p = 3$. To show the improvement by the proposed MSFEM an FEM solution $\mathbf{A}_{\mathrm{FEM}}$ has been calculated using FEs of order $p = 1$. The cell solutions $\mathbf{A}_i$ in the MS approach have been calculated by solving (10) with order $p = 3$. For the part $\mathbf{A}_S$ of the MS solution a FE discretisation of order $p = 1$ has been applied. The only difference between the discrete spaces corresponding to $\mathbf{A}_{\mathrm{FEM}}$ and $\mathbf{A}_{\mathrm{MS}}$ is the additional MS part

$$\sum_{i=1}^{M}\sum_{j=1}^{N} c_{i,j,1}\mathbf{S}_{i,j,1} + c_{i,j,2}\mathbf{S}_{i,j,2}. \tag{16}$$

The degrees of freedom (DoF) for calculating $\mathbf{A}_{\mathrm{ref}}$, $\mathbf{A}_{\mathrm{FEM}}$, and $\mathbf{A}_{\mathrm{MS}}$ with respect to the number of cell domains (N_{CD}) can be seen in Table I.

TABLE I
N_{DoF} FOR $\mathbf{A}_{\mathrm{ref}}$, $\mathbf{A}_{\mathrm{FEM}}$, AND $\mathbf{A}_{\mathrm{MS}}$ WITH RESPECT TO THE NUMBER OF CELL DOMAINS

N_{CD}	1	4	9	16	20
N_{ref}	42,456	87,534	153,936	237,051	287,331
N_{FEM}	10,524	21,658	38,038	58,518	70,924
N_{MS}	10,526	21,666	38,056	58,550	70,964

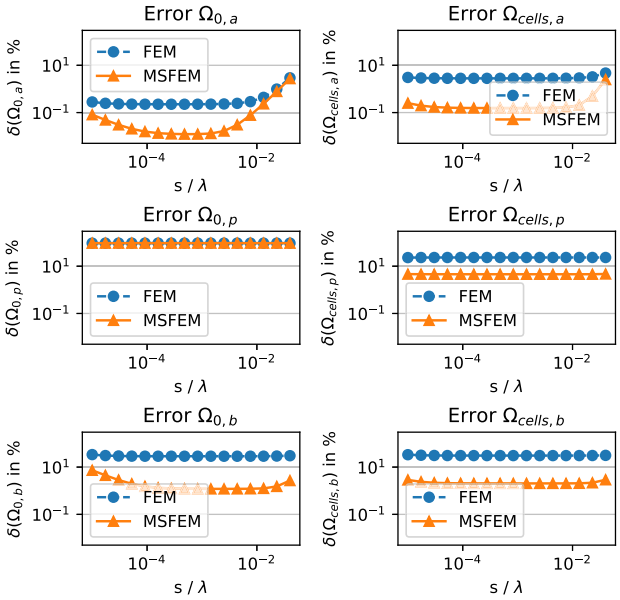

Fig. 5. Relative L^2 error of FEM and MSFEM on the individual subdomains with respect to (s/λ), the ratio of the width of the aperture s to the wavelength λ is shown. The error in the exterior domain Ω_0 is on the left, the error in the combined cell domains Ω_{cells} is on the right, the error above the panel is in the first row, the error in the panel is in the middle row and the error below the panel is in the last row.

The method has been applied to different shapes of apertures which lead to similar results as for the square aperture. The simulations have been carried out with the open-source FE software Netgen/NGSolve [7].

A. MSFEM Varying the Frequency f

The method has been applied for a range of frequencies f between 1.5 MHz and 6 GHz. For the excitation (5) $\alpha = 0$ has been chosen, which corresponds to the wave vector

$$\mathbf{k} = (0, 0, -1)^\top \tag{17}$$

representing a plane wave impinging directly from above. Note, that with this angle homogenous NBCs are set on Γ_{front} and Γ_{back}. On the subdomains the relative L^2 error

$$\delta(\mathbf{A}, \Omega) := \frac{\|\mathbf{A} - \mathbf{A}_{\mathrm{ref}}\|_{\mathrm{L}^2(\Omega)}}{\|\mathbf{A}_{\mathrm{ref}}\|_{\mathrm{L}^2(\Omega)}} \tag{18}$$

with respect to (s/λ), the ratio of the width of the aperture s to the wavelength

$$\lambda = \frac{c_0}{f}, \quad c_0 = \frac{1}{\sqrt{\mu_0\varepsilon_0}} \tag{19}$$

has been evaluated for $\mathbf{A}_{\mathrm{FEM}}$ and $\mathbf{A}_{\mathrm{MS}}$ and can be seen in Fig. 5.

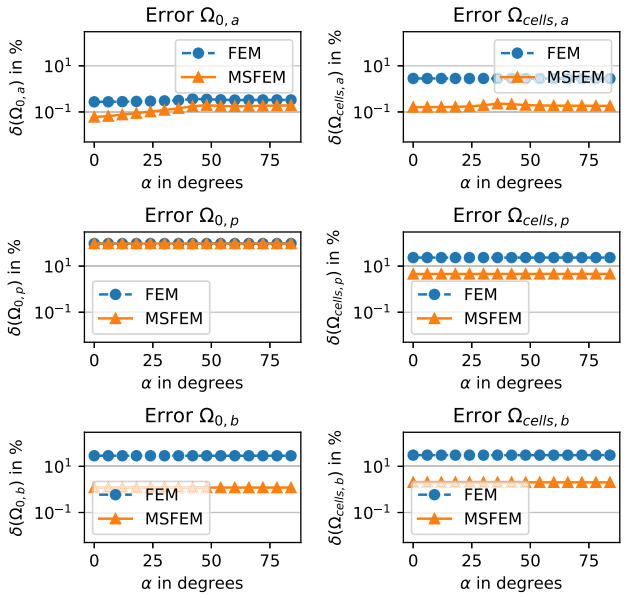

Fig. 6. Relative L^2 error for FEM and MSFEM on the individual parts of the domain with respect to α, the oblique angle of the impinging plane wave, is shown. The error in the exterior domain Ω_0 is on the left, the error in the combined cell domains Ω_{cells} is on the right, the error above the panel is in the first row, the error in the panel is in the middle row, and the error below the panel is in the last row.

The method leads to a substantial improvement in $\Omega_{0,a}$. The solution in $\Omega_{0,a}$ is mainly dominated by the reflection on the panel and less on the reflection and transmission through the apertures. The error in $\Omega_{\text{cells},a}$ is essentially improved because it depends on the reflected and transmitted part through the apertures. The solution in $\Omega_{0,p}$ is not improved. This is expected because the MS functions in the cell domains do not influence the solution significantly in the exterior panel. On the contrary, the method improves the solution in $\Omega_{\text{cells},p}$, because the penetration of the panel is resolved by the MS functions. As expected, the biggest improvements are achieved below the panel. This holds for $\Omega_{\text{cells},b}$ as well as for $\Omega_{0,b}$. The solution below the panel is mainly defined by the transmission through the apertures. The choice of the MS functions as propagating waves from above transmitted through the apertures is essential.

Interesting is the deterioration of the method for low and high frequencies. In the case of low frequencies the panel in the exterior domain $\Omega_{0,p}$ is fully penetrated by the plane wave from above and the field below the panel mainly depends on this transmission. For high frequencies both FEM and MSFEM deteriorate. FEM deteriorates due to the fact that the discrete space does not resolve the wavelength sufficiently anymore. The MSFEM does not improve this and therefore suffers from the same problem.

For a frequency with a wavelength approximately the size of an aperture s, the FE resolution is fine enough so that the MSFEM does not lead to an improvement. The small-scale behavior around the apertures is already resolved by the discretization.

B. MSFEM Varying the Angle α

The angle α of the impinging plane wave has been varied to show the behavior for oblique impinging waves. The boundary conditions depending on α have been chosen according to Section II. A frequency of $f = 1$ GHz has been chosen. The error in the different domains can be seen in Fig. 6.

The MSFEM improves the accuracy of the field below the panel and in $\Omega_{\text{cells},a}$ and $\Omega_{\text{cells},p}$. As expected, no improvement is accomplished in $\Omega_{0,p}$ and only moderate improvement in $\Omega_{0,a}$. Although only MS functions representing plane waves impinging perpendicular from above are used to enhance the space, the method can cope with plane waves from oblique angles.

VI. Conclusion

An MSFEM for wave propagation problems with 3-D ventilation panels considering lossy materials has been introduced. The method improves the accuracy of coarse FE simulations by enhancing the discrete space around the apertures. In this work solutions of small cell domains are used for this purpose. The feasibility of the proposed method is shown by numerical experiments for a wide range of frequencies and for plane waves impinging from oblique angles. Mainly, the solution underneath the panel is essentially improved, but moderate improvements have been observed above the panel and partially inside the panel. It is remarkable that only two MS functions per aperture are necessary for the improvements. Although the MS functions only represent solutions of small problems with impinging plane waves perpendicular to the panel, the accuracy in simulations with plane waves impinging at an oblique angle is improved dramatically.

Acknowledgment

This work was supported by the "University SAL Labs" initiative of Silicon Austria Labs (SAL) and its Austrian partner universities for applied fundamental research for electronic-based systems.

References

[1] C. L. Holloway and E. F. Kuester, "Generalized sheet transition conditions for a metascreen—A fishnet metasurface," *IEEE Trans. Antennas Propag.*, vol. 66, no. 5, pp. 2414–2427, May 2018.
[2] I. Bardi, G. Peng, and L. E. R. Petersson, "Modeling periodic layered structures by shell elements using the finite-element method," *IEEE Trans. Magn.*, vol. 52, no. 3, Mar. 2016, Art. no. 7402004.
[3] K. Hollaus and J. Schöberl, "Some 2-D multiscale finite-element formulations for the eddy current problem in iron laminates," *IEEE Trans. Magn.*, vol. 54, no. 4, pp. 1–16, Apr. 2018.
[4] M. Leumuller, B. Auinger, J. Schoberl, and K. Hollaus, "Enhanced technique for metascreens using the generalized finite element method," *IEEE Trans. Magn.*, vol. 57, no. 6, Jun. 2021, Art. no. 7401704.
[5] A. Chatterjee, J. M. Jin, and J. L. Volakis, "Edge-based finite elements and vector ABCs applied to 3-D scattering," *IEEE Trans. Antennas Propag.*, vol. 41, no. 2, pp. 221–226, Feb. 1993.
[6] J. Schöberl and S. Zaglmayr, "High order Nédélec elements with local complete sequence properties," *COMPEL-Int. J. Comput. Math. Electr. Electron. Eng.*, vol. 24, no. 2, pp. 374–384, Jun. 2005.
[7] J. Schöberl. *Netgen/Ngsolve*. Accessed: Oct. 18th, 2021. [Online]. Available: https://ngsolve.org